

SUPPORTING INFORMATION

Synthesis of stable $\text{Cu}_n\text{Au}_{25-n}$ nanoclusters ($n = 1-9$) using selenolate ligands

Wataru Kurashige,^a Kenta Munakata,^a Katsuyuki Nobusada,^b and Yuichi Negishi*^{a,c}

^a Department of Applied Chemistry, Faculty of Science and ^c Research Institute for Science and Technology, Energy and Environment Photocatalyst Research Division, Tokyo University of Science, 1-3 Kagurazaka, Shinjuku-ku, Tokyo 162-8601, Japan. ^b Department of Theoretical and Computational Molecular Science, Institute for Molecular Science, Myodaiji, Okazaki, Aichi 444-8585, Japan.

I. Experimental Procedures

A. Chemicals

All chemicals were purchased commercially and used as received without further purification. Hydrogen tetrachloroaurate tetrahydrate ($\text{HAuCl}_4 \cdot 4\text{H}_2\text{O}$) was obtained from Tanaka Kikinzoku. Selenium (Se), bromooctane ($\text{C}_8\text{H}_{17}\text{Br}$), copper(II) acetylacetonate ($\text{Cu}(\text{C}_5\text{H}_8\text{O}_2)_2$), barium sulfate (BaSO_4), octanethiol ($\text{C}_8\text{H}_{17}\text{SH}$), tetraoctylammonium bromide ($(\text{C}_8\text{H}_{17})_4\text{NBr}$), sodium tetrahydroborate (NaBH_4), acetonitrile, toluene, dichloromethane (CH_2Cl_2), and acetone were obtained from Wako Pure Chemical Industries. *Trans*-2-[3-(4-*tert*-butylphenyl)-2-methyl-2-propenylidene] malononitrile (DCTB) was purchased from Fluka. Tetrabutylammonium perchlorate ($(\text{C}_4\text{H}_9)_4\text{NClO}_4$) was purchased from Tokyo Kasei. Dioctyl diselenide ($(\text{C}_8\text{H}_{17}\text{Se})_2$) was synthesized in our laboratory.¹ Deionized water with a resistivity of $>18.2 \text{ M}\Omega \cdot \text{cm}$ was used throughout.

B. Synthesis

The $\text{Cu}_n\text{Au}_{25-n}(\text{SeC}_8\text{H}_{17})_{18}$ ($n = 1-9$) series of clusters was synthesized using the same method previously employed to produce $\text{Au}_{25}(\text{SeC}_8\text{H}_{17})_{18}$ (Figure S1(b)),^{1,2} with a slight modification. Firstly, 20 mL of a toluene solution of $(\text{C}_8\text{H}_{17})_4\text{NBr}$ (0.6 mmol) was added to 6.3 mL of an aqueous solution of HAuCl_4 (30 mM, 0.19 mmol). After stirring for 30 min, the aqueous layer was removed and $\text{Cu}(\text{C}_5\text{H}_8\text{O}_2)_2$ was added to the remaining toluene solution. Solutions were prepared using relative molarity ratios between HAuCl_4 and $\text{Cu}(\text{C}_5\text{H}_8\text{O}_2)_2$ of 24:1, 22:3, 20:5, and 18:7. The mixed solution was stirred for 30 min, following which it was combined with 3 mL of an aqueous NaBH_4 solution (2 mmol). After 1 to 2 s, 2.6 mL of a toluene solution containing $(\text{C}_8\text{H}_{17}\text{Se})_2$ (400 μL) was added rapidly.³ Following this addition, the solution immediately changed colour from orange to dark red. The mixture was subsequently stirred for 1 h, after which the organic phase was washed thoroughly with water and dried under vacuum. The product was suspended in acetonitrile and centrifuged at 3500 rpm to remove byproducts such as $(\text{C}_8\text{H}_{17}\text{Se})_2$ and $(\text{C}_8\text{H}_{17})_4\text{NBr}$. Finally, $\text{Cu}_n\text{Au}_{25-n}(\text{SeC}_8\text{H}_{17})_{18}$ was extracted from the dried product using a mixture of acetone and acetonitrile (Table S1). The thiolate-protected $\text{Cu}_n\text{Au}_{25-n}$ clusters ($\text{Cu}_n\text{Au}_{25-n}(\text{SC}_8\text{H}_{17})_{18}$) used for comparison purposes were also synthesized using the same experimental conditions, except that $\text{C}_8\text{H}_{17}\text{SH}$ was used instead of $(\text{C}_8\text{H}_{17}\text{Se})_2$.

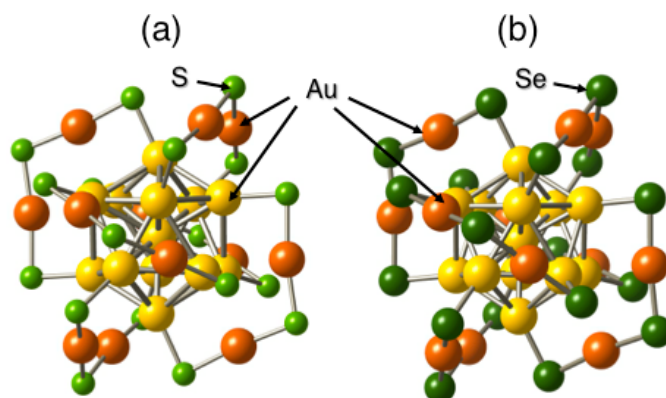


Figure S1. Structural representations of (a) $\text{Au}_{25}(\text{SR})_{18}$ as determined by single-crystal X-ray analysis^{4,5} and (b) $\text{Au}_{25}(\text{SeR})_{18}$ as optimized by DFT calculations² (The R moieties are omitted for clarity).

C. Characterization

Matrix-assisted laser desorption ionization (MALDI) mass spectra were acquired via a linear time-of-flight mass spectrometer (Applied Biosystems, Voyager Linear RD VDA 500) with a nitrogen laser (wavelength: 337 nm) and using DCTB as the MALDI matrix.⁶ The cluster-to-matrix ratio was set to 1:1000. The laser fluence was reduced to the lowest value that enabled the ions to be detected.

Transmission electron microscopy (TEM) images were recorded using an electron microscope (Hitachi, H-7650) operated at 100 kV, typically using a magnification of 100,000.

X-ray photoelectron spectra were collected using an electron spectrometer (JEOL, JPS-9010MC) equipped with a chamber at a base pressure of $\sim 2 \times 10^{-8}$ Torr. X-rays from the Mg-K α line at 1253.6 eV were used for excitation.

X-ray diffraction (XRD) measurements were performed on a diffractometer (Rigaku, Rint2500) using Cu-K α radiation ($\lambda = 1.54 \text{ \AA}$) with a reflection-free silicon plate (Rigaku) as a substrate.

UV-Vis absorption spectra of the clusters were recorded in toluene at ambient temperature with a spectrometer (JASCO, V-630). The wavelength-dependent optical data, $I(w)$, were converted to energy-dependent data, $I(E)$, using the following relation, which conserves the integrated spectral areas.

$$I(E) = I(w)/(\partial E/\partial w) \propto I(w) \times w^2$$

Photoluminescence (PL) spectra of the clusters were recorded in toluene at ambient temperature using a spectrofluorometer (Shimadzu, NIR-PL system), without prior degassing of the sample solutions. The cluster concentrations in solutions used for the PL measurements were $< 10 \mu\text{M}$, since the PL intensities increase linearly with the cluster concentration.

Differential pulse voltammetry (DPV) was performed at room temperature in 0.1 M $(\text{C}_4\text{H}_9)_4\text{NClO}_4$ cluster solutions (10 mg/3 mL) using an electrochemical analyzer (BAS, ALS610D). A glassy carbon working electrode and a Pt wire counter electrode were used and ferrocene was employed as an internal reference.

D. Stability in toluene solution

5 mg of $\text{Cu}_n\text{Au}_{25-n}(\text{SeC}_8\text{H}_{17})_{18}$ or $\text{Cu}_n\text{Au}_{25-n}(\text{SC}_8\text{H}_{17})_{18}$ were dissolved in 10 mL toluene solution, and the solutions were allowed to stand at room temperature (25 °C).

II. Calculations

Density functional theory (DFT) calculations were performed for $[\text{CuAu}_{24}(\text{SeCH}_3)_{18}]$. In these calculations, the experimentally synthesized copper-doped clusters were modeled by replacing the octaneselenolate ligands with methaneselenolate. This simplification of the ligands has frequently been applied in previous calculations and is generally accepted as a reasonable approach.^{7,8} Geometric optimization of the clusters was performed starting from an initial structural estimate based on $\text{Au}_{25}(\text{SeCH}_3)_{18}$,² the structure of which was optimized by DFT calculations in our previous study based on single-crystal X-ray data of $\text{Au}_{25}(\text{SC}_2\text{H}_4\text{Ph})_{18}$.⁴ This initial structure appears to be relatively symmetric; however, we did not assume a high degree of molecular symmetry in our calculations and instead performed full geometry optimization of the cluster. The TURBOMOLE package of *ab initio* quantum chemistry programs⁹ was utilized in all calculations. Geometric optimizations based on a quasi-Newton-Raphson method were performed at the level of Kohn-Sham density functional theory (KS-DFT) employing the hybrid functional (PBE0).¹⁰ The double- ζ valence quality plus polarization basis in the TURBOMOLE basis set library was adopted in the calculations, along with a 60-electron relativistic effective core potential¹¹ for the gold atom. Optimized structures with different doping positions of the center of Au_{13} core (C), the surface of Au_{13} core (S), and the $[-\text{SeR}-\text{Au}-\text{SeR}-\text{Au}-\text{SeR}-]$ oligomer (O) were also obtained at the same level of theory. The absorption spectra were simulated by applying time-dependent KS linear response theory.¹²⁻¹⁴

III. Results

Table S1. Yield of each $\text{Cu}_n\text{Au}_{25-n}(\text{SeC}_8\text{H}_{17})_{18}$ in the product synthesized with $[\text{HAuCl}_4]/[\text{Cu}(\text{C}_5\text{H}_8\text{O}_2)_2] = 18:7$.

Cluster	Yield (%) ^a
$\text{Au}_{25}(\text{SeC}_8\text{H}_{17})_{18}$	1.8
$\text{Cu}_1\text{Au}_{24}(\text{SeC}_8\text{H}_{17})_{18}$	6.0
$\text{Cu}_2\text{Au}_{23}(\text{SeC}_8\text{H}_{17})_{18}$	10.7
$\text{Cu}_3\text{Au}_{22}(\text{SeC}_8\text{H}_{17})_{18}$	17.4
$\text{Cu}_4\text{Au}_{21}(\text{SeC}_8\text{H}_{17})_{18}$	18.3
$\text{Cu}_5\text{Au}_{20}(\text{SeC}_8\text{H}_{17})_{18}$	14.5
$\text{Cu}_6\text{Au}_{19}(\text{SeC}_8\text{H}_{17})_{18}$	10.9
$\text{Cu}_7\text{Au}_{18}(\text{SeC}_8\text{H}_{17})_{18}$	8.3
$\text{Cu}_8\text{Au}_{17}(\text{SeC}_8\text{H}_{17})_{18}$	6.7
$\text{Cu}_9\text{Au}_{16}(\text{SeC}_8\text{H}_{17})_{18}$	5.5

^a Estimated from the relative ion intensities in the mass spectrum.

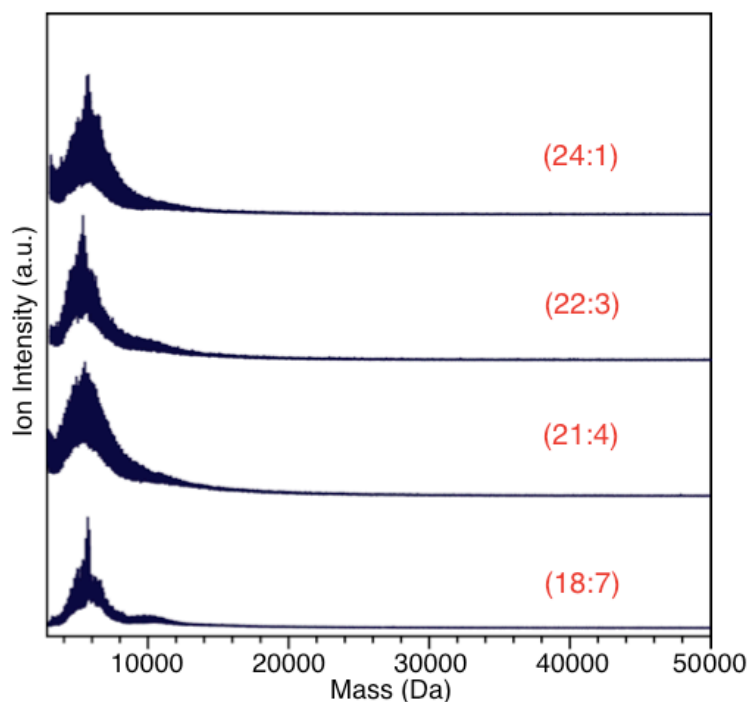


Figure S2. Negative-ion MALDI mass spectra of $\text{Cu}_n\text{Au}_{25-n}(\text{SeC}_8\text{H}_{17})_{18}$ synthesized using different metal ion ratios. These mass spectra were recorded at a high laser fluence for the purpose of observing all the clusters included in the samples. The notation ($N:M$) represents the initial metal ion ratios such that $[\text{HAuCl}_4]:[\text{Cu}(\text{C}_5\text{H}_8\text{O}_2)_2] = N:M$. Laser fragment ions were observed only in the mass region of 4000-8500 Da, indicating that each product contains only the anticipated $\text{Cu}_n\text{Au}_{25-n}(\text{SeC}_8\text{H}_{17})_{18}$.¹

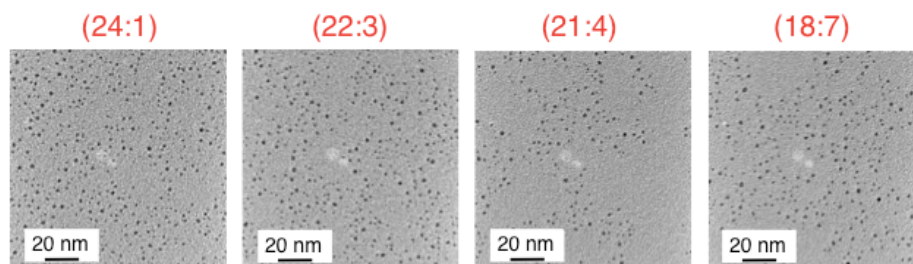


Figure S3. TEM images of $\text{Cu}_n\text{Au}_{25-n}(\text{SeC}_8\text{H}_{17})_{18}$ synthesized at different metal ion ratios. The notation ($N:M$) represents $[\text{HAuCl}_4]:[\text{Cu}(\text{C}_5\text{H}_8\text{O}_2)_2]$.

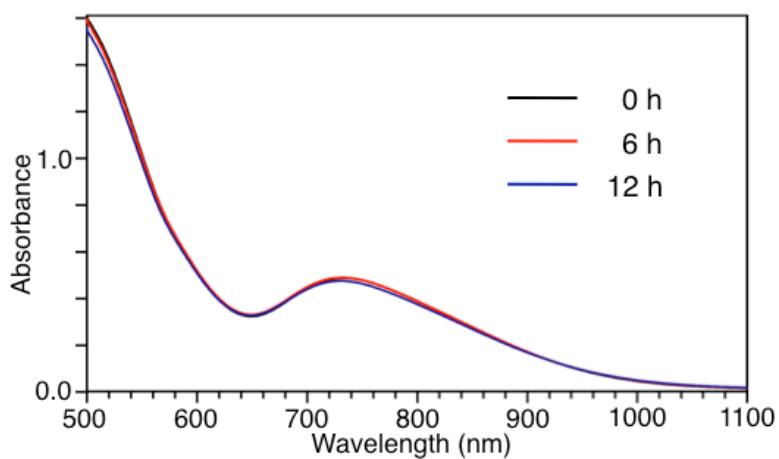


Figure S4. Time dependence of optical absorption spectra of a toluene solution of $\text{Cu}_n\text{Au}_{25-n}(\text{SeC}_8\text{H}_{17})_{18}$ ($n = 0-7$) (see also Figure 2).

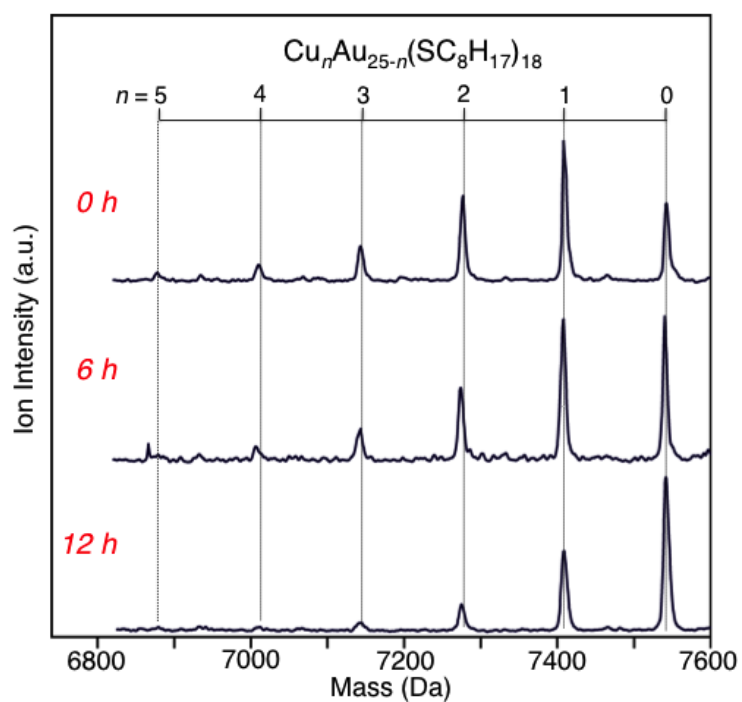


Figure S5. Time-dependent MALDI mass spectra of a toluene solution of $\text{Cu}_n\text{Au}_{25-n}(\text{SC}_8\text{H}_{17})_{18}$ ($n = 0-5$).

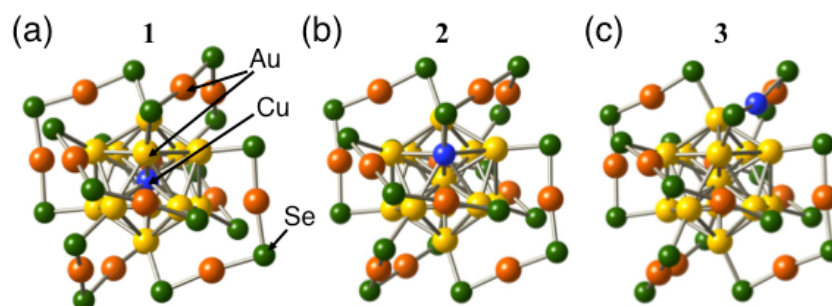


Figure S6. Optimized structures for [CuAu₂₄(SeCH₃)₁₈]⁻ based on (a) center atom doping (1), (b) surface atom doping (2), and (c) oligomer atom doping (3).

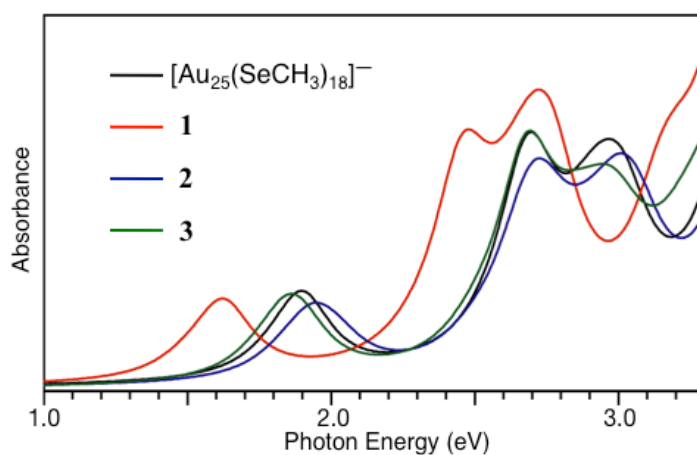


Figure S7. Calculated optical absorption spectra for [Au₂₅(SeCH₃)₁₈]⁻, **1**, **2**, and **3** (see also Figure S6). The overall absorption spectrum of **1** is shifted to a lower energy relative to that of [Au₂₅(SeCH₃)₁₈]⁻ indicating that the HOMO–LUMO gap is reduced (red line). For **2** and **3**, there is almost no change in the absorption spectrum compared to that of [Au₂₅(SeCH₃)₁₈]⁻, showing that the HOMO–LUMO gap has changed very little (blue and green lines, respectively). As shown in Figures 3(a) and S13, the optical absorption spectrum of Cu_nAu_{25-n}(SeC₈H₁₇)₁₈ is shifted to a lower energy relative to that of Au₂₅(SeC₈H₁₇)₁₈, indicating that the HOMO–LUMO gap is reduced. Based on these results, the first copper atom is presumed to be doped to the C cite, as occurs in the case of CuAu₂₄(SC₂H₄Ph)₁₈.¹⁵ However, further studies are needed to allow a more exact determination of the doping site.

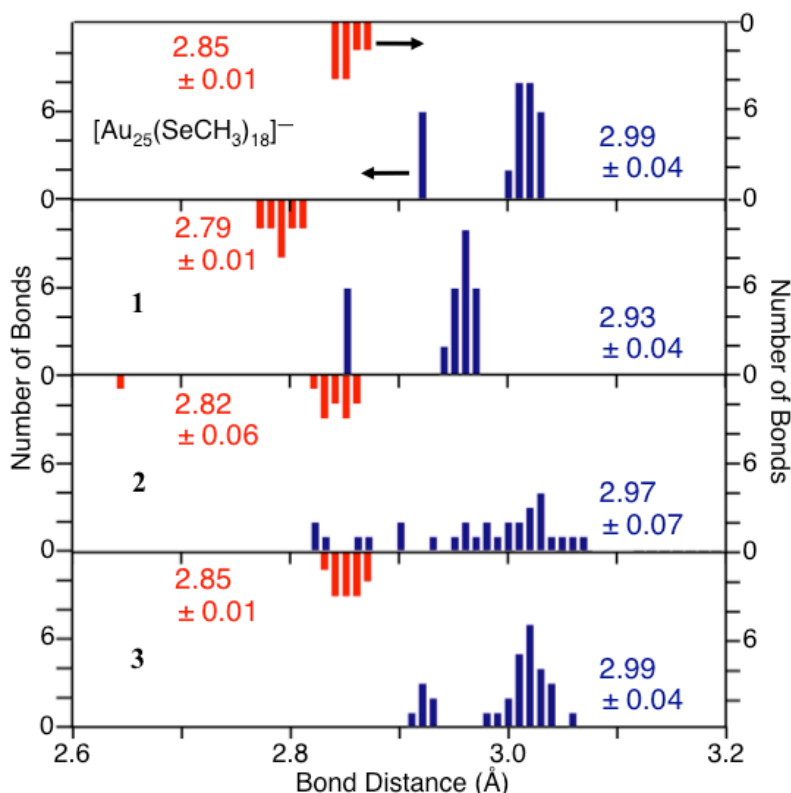


Figure S8. Calculated bond distances in $[\text{Au}_{25}(\text{SeCH}_3)_{18}]^-$, **1**, **2**, and **3** (see also Figure S6). Red: central atom to surface atom. Blue: surface atom to surface atom. Numbers indicate the average and standard deviation of each bond distance. For **1**, both the bond distances between the central atom and surface atoms (red) and those between the surface atoms (blue) are much smaller than those in $[\text{Au}_{25}(\text{SCH}_3)_{18}]^-$, indicating that the metal core contracts in **1**. For **2**, some of the bonds between central atoms and the surface atoms are significantly reduced and the bond distances between the surface atoms are also uneven. These results indicate that the symmetry of the metal core is reduced in **2**. For **3**, there is barely any distortion of the metal core; however, the distances between the metal core and the metal atoms in the oligomers differ (see also Figure S9), indicating that the total symmetry of the cluster is reduced. Thus, the geometric structure of the cluster is significantly distorted when copper is doped at any cluster site. These results are consistent with those obtained for copper doping of $[\text{Au}_{25}(\text{SCH}_3)_{18}]^-$.¹⁵

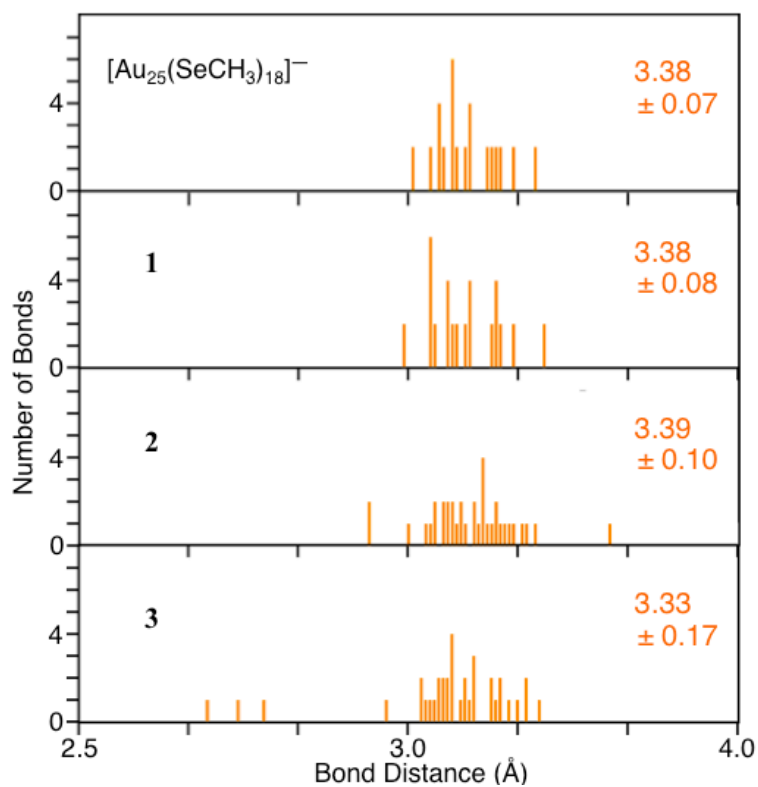


Figure S9. Calculated distances between surface metal atoms (Au or Cu) and metal atoms (Au or Cu) in oligomers in $[\text{Au}_{25}(\text{SeCH}_3)_{18}]^-$, **1**, **2**, and **3**. Numbers indicate average and standard deviation of each distance.

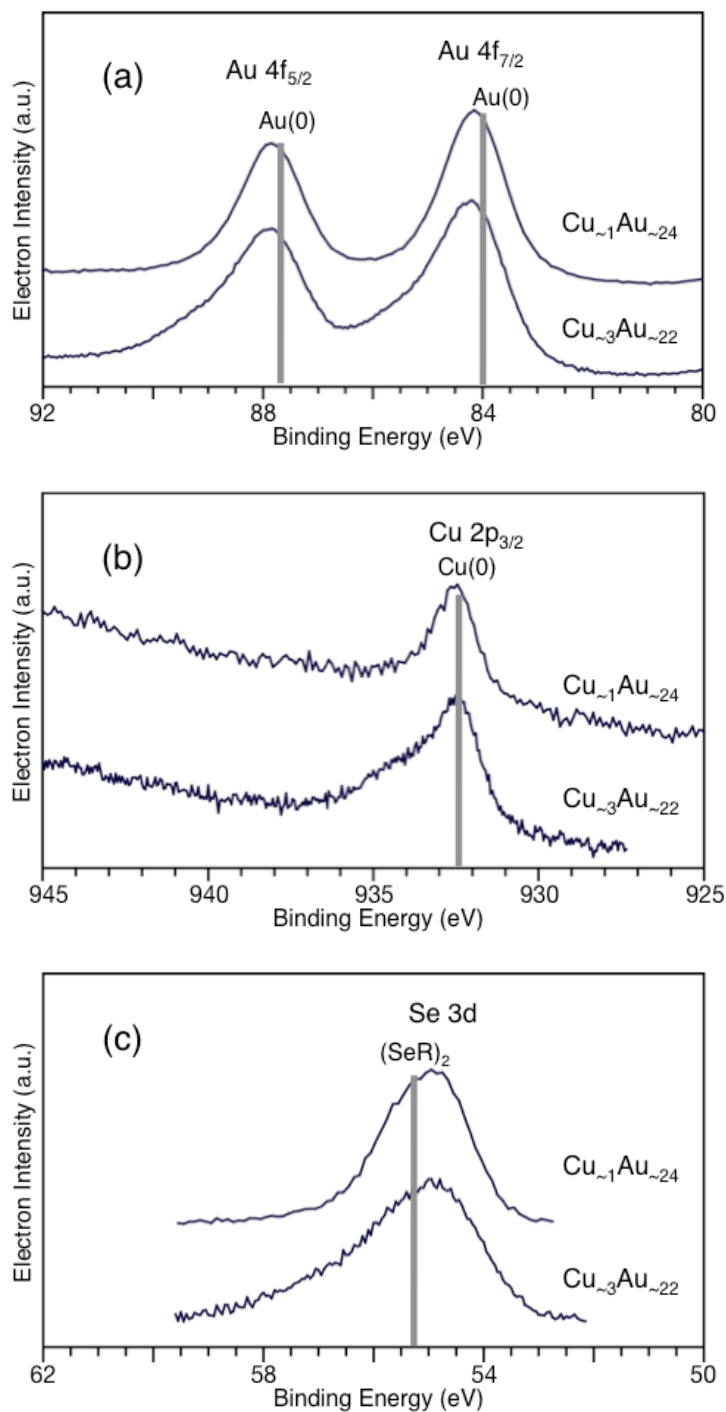


Figure S10. (a) Au 4f spectra, (b) Cu 2p spectra, and (c) Se 3d spectra of $\text{Cu}_{-1}\text{Au}_{-24}(\text{SeC}_8\text{H}_{17})_{18}$ and $\text{Cu}_{-3}\text{Au}_{-22}(\text{SeC}_8\text{H}_{17})_{18}$ (see also Figure 1). In (a)-(c), the binding energies of Au(0) (84.0 and 87.7 eV), Cu(0) (932.4 eV), Cu(II) (933.6 eV), and (SeR)₂ (55.3 eV) are indicated by the grey bars. In (a), Au 4f peaks of $\text{Cu}_{-1}\text{Au}_{-24}(\text{SeC}_8\text{H}_{17})_{18}$ (84.2 and 87.9 eV) and $\text{Cu}_{-3}\text{Au}_{-22}(\text{SeC}_8\text{H}_{17})_{18}$ (84.2 and 87.9 eV) were observed at almost the same energy levels as for $\text{Au}_{25}(\text{SeC}_8\text{H}_{17})_{18}$ (84.2 and 87.9 eV)¹. In (b), Cu 2p peaks (Cu 2p_{3/2} = 932.5 eV) were observed at almost the same energy as for Cu(0) (932.4 eV), which is in contrast to the case of $\text{CuAu}_{24}(\text{SR})_{18}$.¹⁵ In (c), Se 3d peak positions of $\text{Cu}_{-1}\text{Au}_{-24}(\text{SeC}_8\text{H}_{17})_{18}$ (54.9 eV) and $\text{Cu}_{-3}\text{Au}_{-22}(\text{SeC}_8\text{H}_{17})_{18}$ (55.0 eV) were seen at essentially the same energy levels as for $\text{Au}_{25}(\text{SeC}_8\text{H}_{17})_{18}$ (54.9 eV).¹

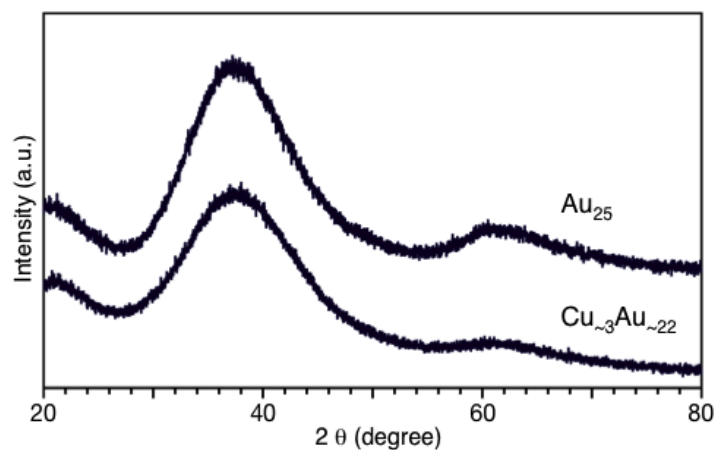


Figure S11. Comparison of the X-ray diffraction patterns of Au₂₅(SeC₈H₁₇)₁₈ and Cu_{~3}Au_{~22}(SeC₈H₁₇)₁₈ (see also Figure 1), demonstrating minimal effects of Cu doping.

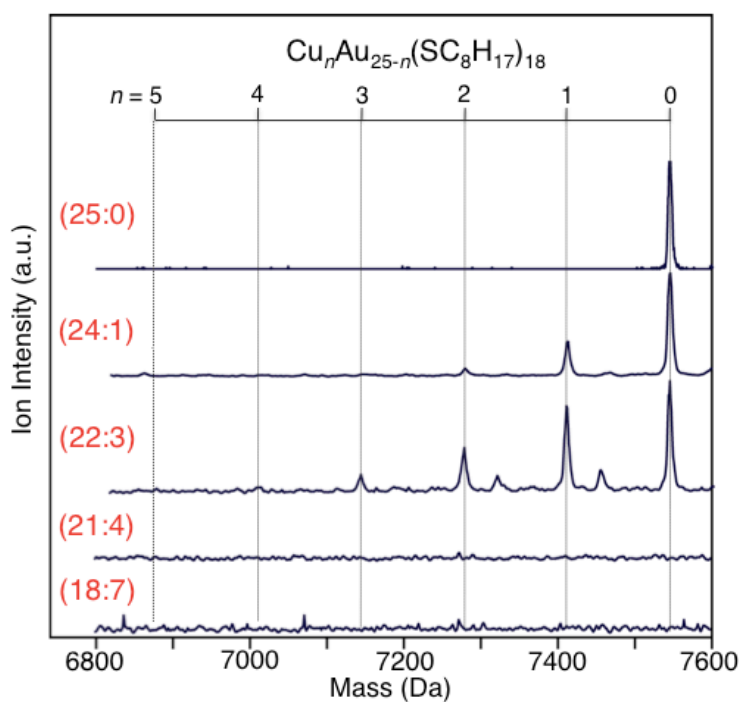


Figure S12. Negative-ion MALDI mass spectra of Cu_nAu_{25-n}(SC₈H₁₇)₁₈ synthesized using the same experimental conditions as Cu_nAu_{25-n}(SeC₈H₁₇)₁₈ except that C₈H₁₇SH was used instead of (C₈H₁₇Se)₂. The notation (*N*:*M*) represents the initial metal ion ratio [HAuCl₄]:[Cu(C₅H₈O₂)₂]. The number of copper atoms in Cu_nAu_{25-n}(SC₈H₁₇)₁₈ varied slightly with the initial [HAuCl₄]:[Cu(C₅H₈O₂)₂] ratio. However, Cu_nAu_{25-n}(SC₈H₁₇)₁₈ containing more than six copper atoms was not obtained at any initial [HAuCl₄]:[Cu(C₅H₈O₂)₂] ratio. Cu_nAu_{25-n}(SC₈H₁₇)₁₈ was not synthesized at [HAuCl₄]:[(C₅H₈O₂)₂] = 21:4 and 18:7. These results are consistent with those of our previous study.¹⁵

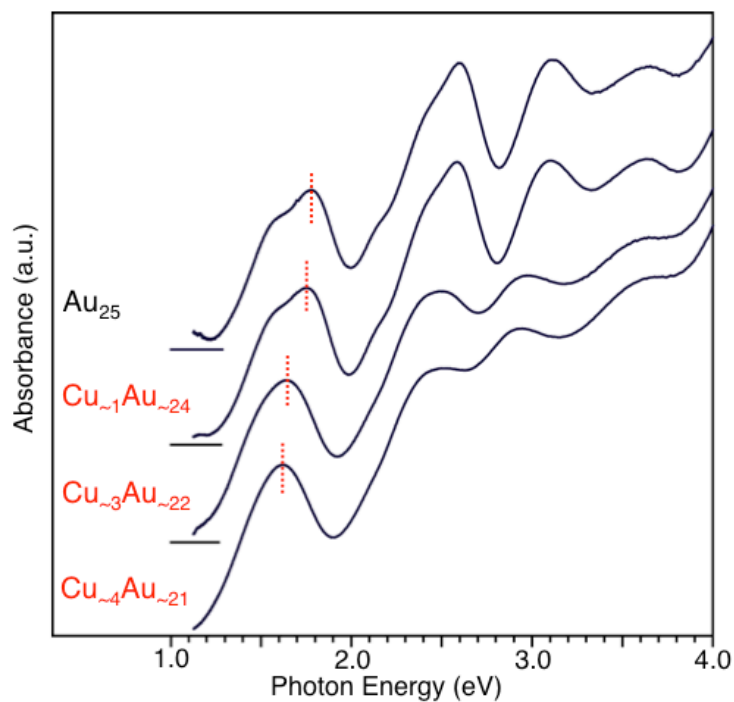


Figure S13. Optical absorption spectra of toluene solutions of $\text{Cu}_n\text{Au}_{25-n}(\text{SC}_8\text{H}_{17})_{18}$ (see also Figures 1 and 3(a)).

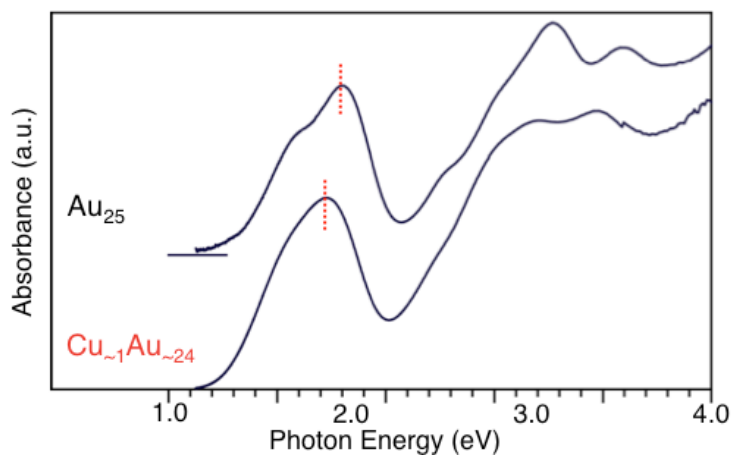


Figure S14. Optical absorption spectra of toluene solutions of $\text{Au}_{25}(\text{SC}_8\text{H}_{17})_{18}$ and $\text{Cu}_{~1}\text{Au}_{~24}(\text{SC}_8\text{H}_{17})_{18}$ with the same chemical composition distribution shown in Figure S5 (at 0 h). The optical absorption spectrum of $\text{Cu}_{~1}\text{Au}_{~24}(\text{SC}_8\text{H}_{17})_{18}$ is shifted to a lower energy relative to that of $\text{Au}_{25}(\text{SC}_8\text{H}_{17})_{18}$, indicating that the HOMO–LUMO gap is reduced (0.08 eV; 20 nm). These results are consistent with our previous study in which $\text{PhC}_2\text{H}_4\text{SH}$ was used as the ligand.¹⁵

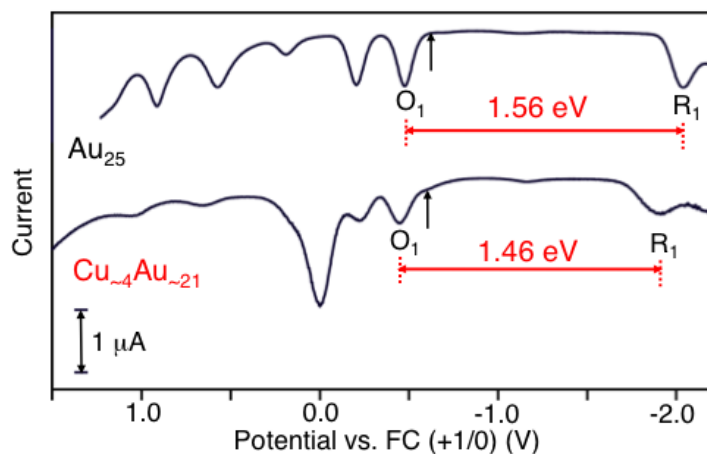


Figure S15. DPV curves of $\text{Au}_{25}(\text{SeC}_8\text{H}_{17})_{18}$ and $\text{Cu}_4\text{Au}_{21}(\text{SeC}_8\text{H}_{17})_{18}$ (see also Figure 1) in CH_2Cl_2 containing 0.1 M $(\text{C}_4\text{H}_9)_4\text{NClO}_4$ (positive scan only). The cluster concentrations were 3.3 mg/mL. Ferrocene was used as an internal reference. O_1 and R_1 indicate the first oxidation and reduction peaks of the clusters, respectively. The black arrows indicate solution open-circuit potentials. The electrochemical HOMO-LUMO gaps¹⁶ of $\text{Au}_{25}(\text{SeC}_8\text{H}_{17})_{18}$ and $\text{Cu}_4\text{Au}_{21}(\text{SeC}_8\text{H}_{17})_{18}$ are estimated to be 1.56 and 1.46 eV, respectively (red arrows).

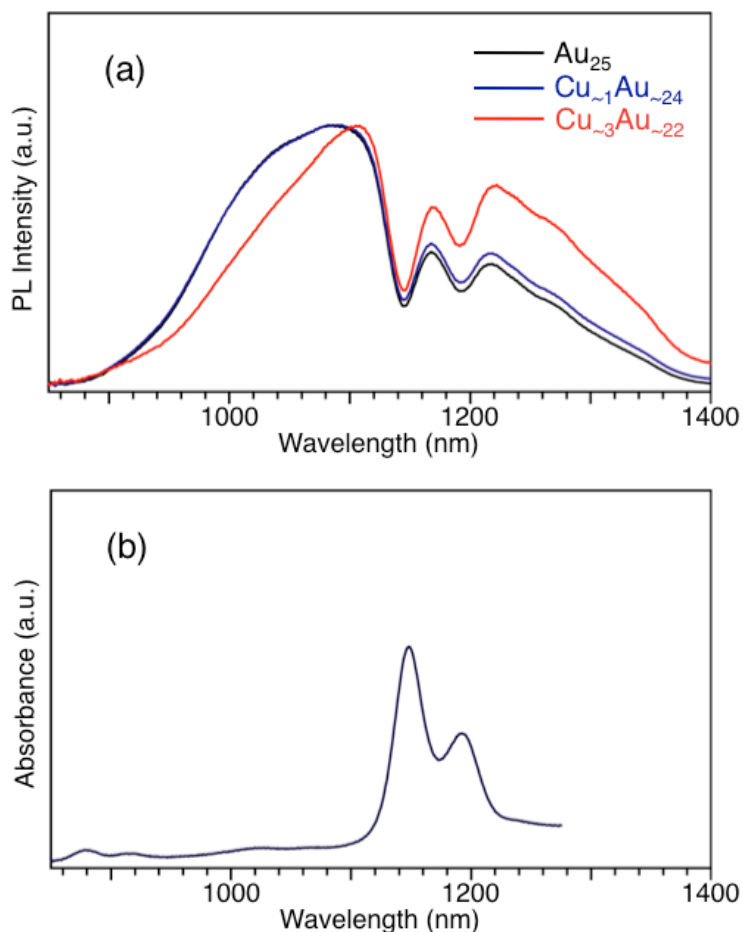


Figure S16. (a) PL spectra of $\text{Cu}_n\text{Au}_{25-n}(\text{SeC}_8\text{H}_{17})_{18}$ with excitation at 400 nm (see also Figure 3(b)) normalized to maximum peak height. The valleys in the region of 1100–1220 nm are due to the absorption by the solvent (toluene). The quantum yields of $\text{Au}_{25}(\text{SeC}_8\text{H}_{17})_{18}$, $\text{Cu}_1\text{Au}_{24}(\text{SeC}_8\text{H}_{17})_{18}$, and $\text{Cu}_3\text{Au}_{22}(\text{SeC}_8\text{H}_{17})_{18}$ are 0.014, 0.012, and 0.008, respectively. (b) Near-infrared absorption spectrum of toluene, obtained by measuring the absorption of BaSO_4 containing a small portion of toluene via spectrometer (JASCO, V-670).

References

1. Y. Negishi, W. Kurashige and U. Kamimura, *Langmuir*, 2011, **27**, 12289–12292.
2. W. Kurashige, M. Yamaguchi, K. Nobusada and Y. Negishi, *J. Phys. Chem. Lett.*, 2012, **3**, 2649–2652.
3. Y. Li, O. Zaluzhna, B. Xu, Y. Gao, J. M. Modest and Y. Y. J. Tong, *J. Am. Chem. Soc.*, 2011, **133**, 2092–2095.
4. M. W. Heaven, A. Dass, P. S. White, K. M. Holt and R. W. Murray, *J. Am. Chem. Soc.*, 2008, **130**, 3754–3755.
5. M. Zhu, C. M. Aikens, F. J. Hollander, G. C. Schatz and R. Jin, *J. Am. Chem. Soc.*, 2008, **130**, 5883–5885.
6. A. Dass, A. Stevenson, G. R. Dubay, J. B. Tracy and R. W. Murray, *J. Am. Chem. Soc.*, 2008, **130**, 5940–5946.
7. K. Nobusada, *J. Phys. Chem. B*, 2004, **108**, 11904–11908.
8. T. Iwasa and K. Nobusada, *J. Phys. Chem. C*, 2007, **111**, 45–49.
9. *TURBOMOLE*, version 6.3, TURBOMOLE GmbH, Karlsruhe, Germany.
10. C. Adamo and V. Barone, *J. Chem. Phys.*, 1999, **110**, 6158–6170.
11. D. Andrae, U. Häussermann, M. Dolg, H. Stoll and H. Preuss, *Theor. Chim. Acta*, 1990, **77**, 123–141.
12. M. E. Casida in *Recent Advances in Density Functional Methods Part I*, ed. D. P. Chong, World Scientific, Singapore, **1995**, vol. 1, pp. 155.
13. R. Bauernschmitt and R. Ahlrichs, *Chem. Phys. Lett.*, 1996, **256**, 454–464.
14. R. Bauernschmitt, M. Häser, O. Treutler and R. Ahlrichs, *Chem. Phys. Lett.*, 1997, **264**, 573–578.
15. Y. Negishi, K. Munakata, W. Ohgake and K. Nobusada, *J. Phys. Chem. Lett.*, 2012, **3**, 2209–2214.
16. K. Kwak and D. Lee, *J. Phys. Chem. Lett.*, 2012, **3**, 2476–2481.